# Seeding of Colloidal Au Nanoparticle Solutions. 2. Improved Control of Particle Size and Shape

Kenneth R. Brown, Daniel G. Walter, and Michael J. Natan*

*Department of Chemistry, Pennsylvania State University, University Park, Pennsylvania 16802*

*Received February 3, 1998. Revised Manuscript Received October 13, 1999*

New fields of research in chemistry and physics require improved synthetic techniques for colloidal metal particles. This paper reports a generally applicable technique for synthesizing colloidal Au particles of mean diameters between 20 and 100 nm that exhibit improved monodispersity relative to previously published methods. In this approach (called "seeding") $Au^{3+}$ is reduced on the surface of preformed 12-nm-diameter Au nanoparticles by introduction of boiling sodium citrate, producing particles highly uniform in size and shape. A similar procedure, utilizing the reductant $NH_2OH$ at room temperature, produces two populations of particles; the larger population is even more spherical than citrate-reduced particles of similar size, while the smaller population is very distinctly rod-shaped.

## Introduction

The use of nanosized colloidal Au nanoparticles has expanded greatly in recent years. Whereas 10−15 years ago, the predominant use of colloidal Au was in biological transmission electron microscopy, a wide variety of recent papers now describe interesting physical properties[1] and possible applications[2] that extend far beyond imaging. For example, Mirkin's group has developed colorimetric DNA sensors based on colloidal Au.[3] Moreover, organized two-dimensional (2-D) and three-dimensional (3-D) arrays of colloidal Au nanoparticles are now occupying the attention of several groups.[4] Unless one studies metal nanoparticles one at a time, as has recently been described,[5] understanding the behavior of solutions and/or surfaces comprising Au nanoparticles is predicated upon having a single size (and shape) of particle because, in the nanometer regime, almost every relevant physical property of colloidal Au is size-dependent.[6] Photolithography[7a] and more recently, nanosphere lithography[7b] has been used to prepare surfaces with highly regular metal features. However, for materials synthesis and for manipulations of these particles in solution,[1−5] nanoparticles prepared from metal ions in solution comprise the preferred starting materials.

Many different preparations have been reported for synthesis of colloidal Au,[1,8] including even some that begin with bulk metal.[9] However, most begin with $Au^{3+}$, and through use of different reductants, generate particles with a range of particle sizes. For example, reducing agents such as $NaBH_4$ or white phosphorus produce small Au particles (diameter < 10 nm) while reductants such as ascorbic acid yield colloidal Au nanoparticles with diameters larger than 10 nm.[10] The

* Author whom all correspondence should be addressed via email at natan@chem.psu.edu.

(1) (a) Kreibig, U.; Vollmer, M. *Optical Properties of Metal Clusters*; Springer-Verlag: Berlin, 1995. (b) Schmid, G. *Chem. Rev.* **1992**, *92*, 1709−1727. (c) Mulvaney, P. *Langmuir* **1996**, *12*, 788−800. (d) Kume, T.; Nakagawa, N.; Hayashi, S.; Yamamoto, K. *Solid State Commun.* **1995**, *93*, 171−175. (e) Farbman, I.; Levi, O.; Efrima, S. *J. Chem. Phys.* **1992**, *96*, 6477−6485. (f) Chernov, S. F.; Zakharov, V. N. *J. Mod. Opt.* **1989**, *36*, 1541−1544. (g) Hache, F.; Ricard, D.; Flytzanis, C.; Kreibig, U. *Appl. Phys. A* **1988**, *47*, 347−357.

(2) (a) Fukumi, K.; Chayahara, A.; Kadono, K.; Sakaguchi, T.; Horino, Y.; Miya, M.; Fujii, K.; Hayakawa, J.; Satou, M. *J. Appl. Phys.* **1994**, *75*, 3075−3080. (b) Lipscomb, L. A.; Nie, S.; Feng, S.; Yu, N.-T. *Chem. Phys. Lett.* **1990**, *170*, 457−461. (c) Angel, S. M.; Katz, L. F.; Archibald, D. D.; Honigs, D. E. *Appl. Spectrosc.* **1989**, *43*, 367−372. (d) Kneipp, K.; Dasari, R. R.; Wang, Y. *Appl. Spectrosc.* **1994**, *48*, 951−955.

(3) (a) Elghanian, R.; Storhoff, J. J.; Mucic, R. C.; Letsinger, R. L.; Mirkin, C. A. *Science* **1997**, *277*, 1078−1081. (b) Storhoff, J. L.; Elghanian, R.; Mucic, R. C.; Mirkin, C. A.; Letsinger, R. L. *J. Am. Chem. Soc.* **1998**, *120*, 1959−1964.

(4) (a) Andres, R. P.; Bielefeld, J. D.; Henderson, J. I.; Janes, D. B.; Kolagunta, V. R.; Kubiak, C. P.; Mahoney, W. J.; Osifchin, R. G. *Science* **1996**, *273*, 1690−1693. (b) Brust, M.; Walker, M.; Bethell, D.; Schiffrin, D. J.; Whyman, R. *J. Chem. Soc., Chem. Commun.* **1994**, 801−802. (c) Giersig, M.; Mulvaney, P *Langmuir* **1993**, *9*, 3408−3413. (d) Alivisatos, A. P.; Johnson, K. P.; Peng, X.; Wilson, T. E.; Loweth, C. J.; Bruchez, M. P., Jr.; Schultz, P. G. *Nature* **1996**, *382*, 609. (e) Harfenist, S. A.; Wang, Z. L.; Alvarez, M. M.; Vezmar, I.; Whetten, R. L. *J. Phys. Chem.* **1995**, *100*, 13904−13910. (f) Mirkin, C. A.; Letsinger, R. L.; Mucic, R. C.; Storhoff, J. J. *Nature* **1996**, *382*, 607. (g) Rubin, S.; Bar, G.; Taylor, T. N.; Cutts, R. W.; Zawodzinski, Jr., T. A. *J. Vac. Sci. Technol. A* **1996**, *14*, 1870−1877. (h) Feldstein, M. J.; Keating, C. D.; Liau, Y.-H.; Natan, M. J.; Sherer, N. F. *J. Am. Chem. Soc.* **1997**, *119*, 6638−6647. (i) Grabar, K. C.; Smith, P. C.; Musick, M. D.; Davis, J. A.; Walter, D. G.; Jackson, M. A.; Guthrie, A. P.; Natan, M. J. *J. Am. Chem. Soc.* **1996**, *118*, 1148−1152.

(5) (a) Emory, S. R.; Nie, S. *Science* **1997**, *275*, 1102−1106. (b) Emory, S. R.; Nie, S. *Anal. Chem.* **1997**, *69*, 2631−2635. (c) Klein, D. L.; McEuen, P. L.; Bowen, J. E.; Roth, R.; Alivisatos, A. P. *Appl. Phys. Lett.* **1996**, *68*, 2574−2576.

(6) (a) Freund, P. L.; Spiro, M. *J. Phys. Chem.* **1985**, *89*, 1074−1077. (b) Zeman, E. J.; Schatz, G. C. *J. Phys. Chem.* **1987**, *91*, 634−643. (c) Quinten, M.; Kreibig, U. *Surf. Sci.* **1986**, *172*, 557−577.

(7) (a) Liao, P. F.; Bergman, J. G.; Chemla, D. S.; Wokaun, A.; Melngailis, J.; Hawyrluk, A. M.; Economou, N. P. *Chem. Phys. Lett.* **1981**, *82*, 355−359. (b) Hulteen J. C.; Van Duyne, R. P. *J. Vac. Sci. Technol., A* **1995**, *13*, 1553−8.

(8) (a) Torigoe, K.; Esumi, K. *Langmuir* **1992**, *8*, 59−64. (b) Esumi, K.; Sato, N.; Torigoe, K.; Meguro, K. *J. Colloid Interface Sci.* **1992**, *149*, 295−298. (c) Leff, D. V.; Ohara, P. C.; Heath, J. R.; Gelbart, W. M. *J. Phys. Chem.* **1995**, *99*, 7036−7041. (d) Duff, D. G.; Baiker, A. *Langmuir* **1993**, *9*, 2301−2309. (e) Duff, D. G.; Baiker, A. *Langmuir* **1993**, *9*, 2310−2317.

(9) (a) Beans, H. T.; Eastlack, H. E. *J. Am. Chem. Soc.* **1915**, *37*, 2667−2683. (b) Nedderson, J.; Chumanov, G.; Cotton, T. M. *Appl. Spectrosc.* **1993**, *47*, 1959−1964.

10.1021/cm980065p CCC: $19.00 
Published on Web 12/29/1999

most widely studied reductant is sodium citrate;[1,11] by varying the citrate:Au ratio, it is possible to prepare colloidal particles with diameters (d) ranging from 10 to 150 nm.[12] Unfortunately, for $d > 30$ nm, the monodispersity becomes poor and the ellipticity ($G$)—the ratio of the major to minor axis—significantly exceeds unity, the value for a sphere. As a result, these particles are of limited value for nanometer-scale architecture. Indeed, of the many published routes to colloidal Au, none produce large (>50 nm) particles with good monodispersity. Their utility is further restricted by the low particle concentrations generated by these methods.

We describe herein the synthesis and characterization of large colloidal Au particles prepared by the "seeding" approach, an adaptation of a method described in the patent literature.[13] In the reported method, 2.6-nm-diameter colloidal Au nanoparticles ("seeds") prepared by $BH_4^-$ reduction are grown to larger sizes by addition of a boiling solution of $HAuCl_4$ and citrate. This approach produces large colloidal Au particles more predictably and reproducibly than citrate reduction, but because the seeds are highly polydisperse (40% standard deviation), the monodispersity is comparable. We reasoned that use of more monodisperse seeds (e.g., 12 ± 1.5 nm diameter) should yield larger particles particles with narrower size distributions, a notion confirmed by experiment. We also describe a superior new synthetic protocol, based on room-temperature seeding of colloidal Au by $NH_2OH/Au^{3+}$.[14,15] This method is consistent and reproducible enough to predict, a priori, final colloidal diameters within a few nanometers. Iterative seeding using this approach can be used to rapidly produce large colloidal Au nanoparticle solutions that exhibit excellent monodispersity. Interestingly, repetitive seeding with $NH_2OH$ leads to formation of a small percentage of cylindrical, high aspect ratio rods. Note that such rods have been generated electrochemically in the pores of membranes.[16,17]

## Experimental Section

**Materials.** $HAuCl_4$, $Na_3$citrate, $NaBH_4$, HCl, $HNO_3$, $H_2SO_4$, and aqueous $H_2O_2$ were obtained from Sigma-Aldrich, Fisher (Acros), or VWR and used without further purification. $H_2O$ was >18 MΩ from a Barnstead Nanopure water purification system.

**Methods.** General protocols for synthesis, characterization, handling, and storage of colloidal Au solutions—including for 17 nM, 12-nm-diameter particles—have been previously described.[18] Samples for atomic absorption (AA) were prepared by digesting 0.1 mL of colloidal Au solution with 30 μL of concentrated $HNO_3$ and 30 μL of concentrated HCl, and diluted to 10 mL. A total of 0.1 mL of this solution was mixed with 0.1 mL of 2% $HNO_3$ and 0.8 mL of $H_2O$ for analysis. Standards were prepared from a 100 ppm stock solution of Au ion (Perkin-Elmer), from which 0.1 mL was mixed with 0.1 mL of 30 μL of $HNO_3$/30 μL of HCl and diluted to 10 mL. Different volumes of 1 ppm stock were mixed with 0.1 mL of 2% $HNO_3$ and diluted to 1.0 mL to yield standards between 25 and 200 ppb. AA samples were burned at 130 °C for 60 s, 1000 °C for 45 s, and atomized at 1800 °C with a 5-s reading window. No salt interference was observed.

*The 2.6-nm-Diameter Colloidal Au.* One milliliter of 1% $HAuCl_4$ was added to 90 mL of $H_2O$ at room temperature (20–23 °C). After 1 min of stirring, 2.00 mL of 38.8 mM sodium citrate was added. One minute later, 1.00 mL of fresh 0.075% $NaBH_4$ in 38.8 mM sodium citrate was added. The colloidal solution was stirred for an additional 5 min and stored in a dark bottle at 4 °C.

*Citrate-Seeded Colloidal Au.* To a stirred solution of boiling 0.01% $HAuCl_4$, seed colloids (either 2.6-nm-diameter or 12-nm-diameter) were added coincidentally with the addition of 38.8 mM sodium citrate (final concentration = 0.17 mM). This mixture was boiled for 15 min and stirred for an additional 10 min while cooling. Citrate-seeded colloids were prepared in volumes ranging from 50 mL to 500 mL, with different diameters were generated by changing the volume of seed colloid added.

*$NH_2OH$-Seeded Colloidal Au.* These syntheses utilized stock solutions of 1% $HAuCl_4$ and 40 mM $H_2NOH$, diluted to final concentrations as described in the figure captions. Except where noted, seed particles were added to stirred mixtures of $NH_2OH$ and $HAuCl_4$.

**Instrumentation.** Optical spectra were obtained on an HP8452A diode array UV–vis spectrophotometer with a deuterium lamp (350–820-nm range, 2-nm resolution). Graphite furnace atomic absorption was performed with a Perkin-Elmer 1100B spectrophotometer, an HGA 700 power supply, an AS-70 autosampler and a Au lamp (Perkin-Elmer). Equipment and protocols for acquisition and analysis of transmission electron microscopy (TEM) images have been described elsewhere.[18,19] Software protocols that allowed 2-D clusters of particles to be separated into individual entities (or when this was not possible, eliminated from consideration) were employed.

## Results and Discussion

**Citrate Seeding.** As part of a study aimed at preparation of protein:Au colloid complexes, a thorough study of the physical properties Au nanoparticles made by the Frens method (i.e., direct reduction of $Au^{3+}$ by citrate[12]) has been published.[20] By varying the citrate:$Au^{3+}$ ratio, Au nanoparticles with diameters from 10 to 70 nm were prepared and characterized by TEM and UV–vis spectrophotometry. Four parameters were used to describe each preparation of colloid: the wavelength

(10) Slot, J. W.; Geuze, H. J. *J. Cell Biol.* **1981**, *90*, 533–536.
(11) Turkevich, J.; Hillier, J.; Stevenson, P. C. *Discuss. Faraday Soc.* **1951**, *11*, 55.
(12) (a) Frens, G. *Nature* **1972**, *241*, 20–22. (b) Frens, G. *Kolloid-Z. u. Z. Polymere* **1972**, *250*, 736–741.
(13) Schutt, E. G. Eur. Patent Application 90317671.4, filed September 25, 1990.
(14) Stremsdoerfer, G.; Perrot, H.; Martin, J. R.; Clechet, P. *J. Electrochem. Soc.* **1988**, *135*, 2881–2885.
(15) Brown, K. R.; Natan, M. J. *Langmuir* **1998**, in press.
(16) Martin, C. R. *Science* **1994**, *266*, 1961–1966. (b) Foss, C. A.; Tierney, M. J.; Martin, C. R. *J. Phys. Chem.* **1992**, *96*, 9001–9007. (c) Hornyak, G. L.; Patrissi, C. J.; Martin, C. R. *J. Phys. Chem.* **1997**, *101*, 1548–1555. (d) Foss, C. A.; Nornyak, G. L.; Stockert, J. A.; Martin, C. R. *J. Chem. Phys.* **1994**, *98*, 2963–2971.
(17) (a) Al-Mawlawi, D.; Liu, C. Z.; Moskovits, M. *J. Mater. Res.* **1994**, *9*, 1014–18. (b) Preston, C. K.; Moskovits, M. *J. Phys. Chem.* **1993**, *97*, 8495–8503.
(18) (a) Grabar, K. C.; Freeman, R. G.; Hommer, M. B.; Natan, M. J. *Anal. Chem.* **1995**, *67*, 735–743. (b) Bright, R. M.; Walter, D. G.; Musick, M. D.; Jackson, M. A.; Allison, K. J.; Natan, M. J. *Langmuir* **1996**, *12*, 810–817. (c) Freeman, R. G.; Grabar, K. C.; Allison, K. J.; Bright, R. M.; Davis, J. A.; Guthrie, A. P.; Hommer, M. B.; Jackson, M. A.; Smith, P. C.; Walter, D. G.; Natan, M. J. *Science* **1995**, *267*, 1629–1632. (d) Grabar, K. C.; Allison, K. J.; Baker, B. E.; Bright, R. M.; Brown, K. R.; Freeman, R. G.; Fox, A. P.; Keating, C. D.; Musick, M. D.; Natan, M. J. *Langmuir* **1996**, *12*, 2353–2361.
(19) Grabar, K. C.; Brown, K. R.; Keating, C. D.; Stranick, S. J.; Tang, S.-L.; Natan, M. J. *Anal. Chem.* **1997**, *69*, 417–477.
(20) (a) Goodman, S. L.; Hodges, G. M.; Trejdosiewicz, L. K.; Livingston, D. C. *J. Microsc.* **1981**, *123*, 201–213. (b) Faulk, W. P.; Taylor, G. M. *Immunochemistry* **1971**, *8*, 1081–1083. (c) Horisberger, M. *Biol. Cell.* **1979**, *36*, 253–258. (d) Hayat, M. A., Ed.; *Colloidal Gold: Principles, Methods, and Applications*; Academic Press: San Diego, 1989; Vols. 1 and 2. (e) Beesley, J. E. *Colloidal Gold: A New Perspective for Cytochemical Marking*; Oxford University: Oxford, 1989; Vol. 17.

**Table 1. Physical Properties of Colloidal Au Nanoparticles Prepared by Direct Citrate Reduction and by Citrate Seeding of 2.6-nm-Diameter and 12-nm-Diameter Colloidal Au Solutions**

| | batch | major axis × minor axis[a] | $G^b$ | $\lambda_{max}$ (nm) | peak width (nm) | source of colloid |
|---|---|---|---|---|---|---|
| small seeds | | 2.6 (1.0) × 2.0 (0.8) | 1.30 | 514 | 104 | this work |
| large seeds | | 12.6 (1.1) × 11.5 (1.0) | 1.10 | 518 | 84 | this work |
| **Synthetic Method** | | | | | | |
| direct citrate | 1 | 21 (2.3) × 19 (2.3)[c] | 1.13 | 524 | 83 | ref 20 |
| | 2 | 22.3 (5.0) × 18.6 (2.4) | 1.20 | 528 | 116 | this work |
| | 3 | 25 (3.3) × 21 (3.3) | 1.19 | 524 | 90 | ref 20 |
| | 4 | 31.7 (7.6) × 24.5 (3.9) | 1.29 | 530 | 136 | this work |
| | 5 | 35 (4.0) × 26 (4.0) | 1.33 | 530 | 108 | ref 20 |
| | 6 | 44 (6.9) × 33 (6.9) | 1.34 | 528 | 104 | ref 20 |
| | 7 | 44.9 (9.5) × 36.4 (5.6) | 1.23 | 524 | 118 | this work |
| | 8 | 48 (10.5) × 37 (10.5) | 1.31 | 535 | 98 | ref 20 |
| | 9 | 56 (8.4) × 41 (8.4) | 1.37 | 535 | 147 | ref 20 |
| seeded, large | 1 | 19.3 (1.7) × 16.4 (1.1) | 1.18 | 520 | 84 | this work |
| | 2 | 21.4 (2.6) × 18.5 (1.9) | 1.16 | 522 | 80 | this work |
| | 3 | 25.0 (2.2) × 21.3 (1.6) | 1.17 | 524 | 80 | this work |
| | 4 | 28.7 (2.6) × 24.3 (2.0) | 1.18 | 526 | 76 | this work |
| | 5 | 31.1 (3.5) × 26.0 (2.4) | 1.20 | 526 | 82 | this work |
| | 6 | 38.4 (4.7) × 31.8 (2.7) | 1.21 | 528 | 78 | this work |
| | 7 | 44.5 (5.8) × 36.8 (4.1) | 1.21 | 530 | 84 | this work |
| | 8 | 53 (4.8) × 43 (3.1) | 1.23 | 534 | 92 | this work |
| | 9 | 64 (6.3) × 51 (3.8) | 1.26 | 545 | 112 | this work |
| | 10 | 72 (9.4) × 54 (5.2) | 1.33 | 542 | 152 | this work |
| | 11 | 76 (11) × 56 (6.0) | 1.36 | 538 | 116 | this work |
| | 12 | 91 (14) × 68 (8.2) | 1.35 | 550 | 220 | this work |
| seeded, small | 1 | 35.8 (8.7) × 30.6 (7.3) | 1.17 | 548 | 188 | this work |
| | 2 | 36.4 (5.2) × 29.6 (3.1) | 1.23 | 530 | 96 | this work |
| | 3 | 43.0 (7.8) × 36.8 (6.2) | 1.17 | 534 | 132 | this work |
| | 4 | 53 (5.2) × 44 (3.7) | 1.21 | 542 | 108 | this work |
| | 5 | 56 (7.2) × 45 (4.6) | 1.25 | 544 | 144 | this work |
| | 6 | 61 (10) × 49 (7.5) | 1.24 | 548 | 164 | this work |
| | 7 | 75 (17) × 60 (11) | 1.24 | 548 | 216 | this work |
| | 8 | 93 (20) × 68 (11) | 1.37 | 572 | 300 | this work |
| | 9 | 108 (38) × 77 (20) | 1.40 | 548 | 300 | this work |
| | 10 | 111 (27) × 81 (17) | 1.38 | 616 | 404 | this work |

[a] Values in parentheses are standard deviations; all values are in nanometers. [b] Ellipticity, as defined in text. [c] Reference 19 gives a single standard deviation for a given preparation of particles, so it is used for both axes.

of maximum absorbance ($\lambda_{max}$) and peak width at half max (PWHM) from the UV−vis data, and the mean particle diameter ($d$) and ellipticity ($G$) from TEM data. Due to the asymmetry of the colloidal Au surface plasmon band,[2a] PWHM is defined straightforwardly as twice the difference between $\lambda_{max}$ and the $\lambda$ of half-maximal absorbance to the red of the $\lambda_{max}$.

In contrast, the mean particle diameter $d$ is an oversimplification in that no colloidal Au particles are purely spherical: TEM images show the presence of major and minor axes (the ellipticity $G$ is the ratio major:minor axial ratio).[19] Accordingly, while $d$ is used herein in reference to the dimensions of the major axis, all particles are described by mean major and minor axes (e.g., Table 1). The TEM images only two of the three dimensions in a particle, and it is assumed that the dimensions of the third are the same as one of the two imaged. The question arises as to whether the particles are prolate (cigar-shaped; third axis = minor) or oblate (pancake-shaped; third axis = major). While Goodman et al.[20] state that colloidal Au nanoparticles are oblate, both logic and experiment suggest that the reverse is true: particles on TEM grids adsorb so as maximize their contact with the surface, meaning the axis normal to the surface must be minor. Since minor and major axes are seen in TEM images, there must be two minor axes, making the particles prolate. In accord with this reasoning, atomic force microscopy images of Au nanoparticles on glass slides known to have axes of 40 and 30 nm indicates the tops of the particles are 30 nm above the surface.[21]

We have compared $d$, $G$, $\lambda_{max}$, and PWHM for Au nanoparticles made by the Frens method to those prepared by seeding (Figure 1 and Table 1). In the approach described in the patent literature,[13] the dimensions of existing Au nanoparticles (the "seeds") are increased by mixing with additional reductant (i.e., citrate) and $Au^{3+}$. In practice, a mixture of citrate and colloidal Au is added to a solution of boiling, dilute $HAuCl_4$ in $H_2O$. What makes this method succeed (or fail) is the relative rate of new particle formation (via $Au^{3+}$ reduction) in solution versus the rate of $Au^{3+}$ reduction on the surface of existing particles. If the latter is much greater than the former, then particle growth will occur at the expense of new particle nucleation. From the volumes of work on production of colloidal Au nanoparticles for biological applications,[1] it is well-appreciated that reduction of $Au^{3+}$ on *any* small particles is rapid, explaining the need for filtered solutions and scrupulously clean glassware for the production of colloidal Au. It is thus reasonable to assume that new particle nucleation can be averted by seeding. The absence of new particle nucleation is especially critical for growth of large particles, because in the Frens method, as particles are growing larger, new (small) particles can be forming.

(21) Lyon, L. A.; Natan, M. J. Unpublished results.

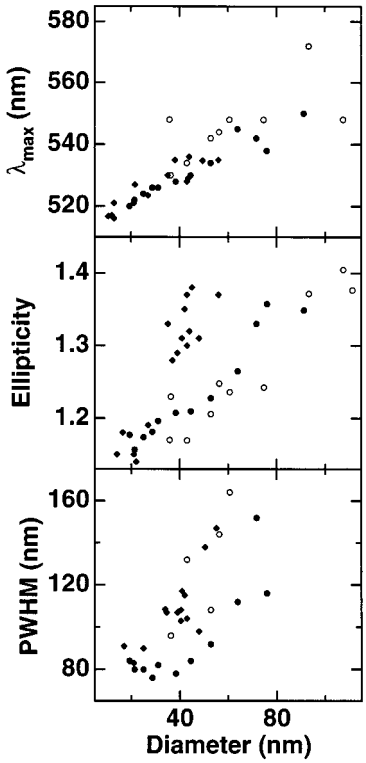


**Figure 1.** Comparison of $\lambda_{max}$ (top), ellipticity ($G$) (middle), and peak width at half-max (PWHM) (bottom) versus major axis diameter for colloidal Au nanoparticles prepared by direct citrate reduction of $Au^{3+}$ (◆) and by citrate-based seeding of 2.6-nm-diameter (○) and 12-nm-diameter (●) colloidal Au.

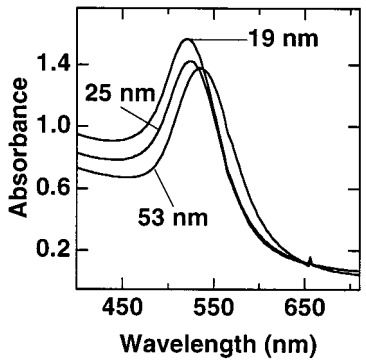


**Figure 2.** Optical spectra for solutions of 19-, 25-, and 53-nm-diameter Au nanoparticles grown by citrate seeding of 12-nm-diameter colloidal Au. Size and shape data for these particles are described in Table 1.

Several general trends are evident by inspection of plots of $\lambda_{max}$, ellipticity, and peak width at half-maximum (PWHM) versus particle diameter for colloidal Au made by Frens' method and by seeding using 2.6- and 12-nm-diameter seeds (Figure 1). For each type of particle, $\lambda_{max}$ increases with increasing size, although not dramatically. Increasing the diameter of a colloidal Au nanoparticle from 19 to 53 nm, nearly a factor of 3, leads only to a 14-nm red shift in $\lambda_{max}$ (Figure 2); red shifts of 150 nm or more can be realized by aggregation of small particles.[18] However, increasing particle diameters lead to increasing ellipticities and to significantly broadened optical spectra. The latter has been shown to result in large part from Rayleigh light scattering from particles with diameters $> \lambda/20$.[22] It should be noted that because light scattering is so sensitive to particle diameter,[23] PWHM can be used as a rapid diagnostic for the quality of citrate-derived, small diameter colloidal Au preparations. For example, in our experience, preparations of 12-nm-diameter colloidal Au with PWHM >85 nm invariably exhibit roughly 2-fold higher standard devations in d than those with PWHM <85 nm (and are thus usually discarded).

Comparison of the physical properties of colloidal Au prepared by seeding with that made by direct citrate reduction indicates the superiority of the former (Table 1). In particular, $G$ is significantly greater for colloidal Au made by direct citrate reduction: several batches clustered around $d = 40$ nm all had $G \geq 1.3$, while the analogous particles made by seeding exhibited $G$ values $\approx 1.2$. Even particles in the 20−30 nm diameter range made by direct citrate reduction were more elliptical than the corresponding seeded particles. Moreover, PWHM for seeded particles are consistently lower than for particles made by direct citrate reduction. For the three sizes of 12-nm seeded particles shown in Figure 2, the PWHM are nearly identical, and the only significant difference is the aforementioned shift in $\lambda_{max}$. Colloidal Au solutions made by direct citrate reduction exhibit broadened PWHM over the entire range of particle diameters.

The high degree of ellipticity in colloidal Au made by direct citrate reduction arises from two components: differential reduction rates at sites on the particle, and differential diffusion to parts of the particles. High-resolution TEM studies have invariably shown the presence of crystalline faces in small colloidal Au nanoparticles.[24] If reduction of $Au^{3+}$ is substantially faster (or slower) on certain faces than on others, then anisotropic particle growth can be expected. In this regard, Wokaun has shown that under certain conditions, highly anisotropic colloidal Au nanoparticles can be prepared;[25] likewise, production of cubic colloidal particles has recently been described.[26] Another factor that could favor elliptical particles is the enhanced amount of $Au^{3+}$ reaching the ends of the ellipse: flux to a hemisphere is enhanced relative to flux to a plane.[27] While this factor is more important in unstirred solutions, even in stirred solutions it could contribute to increased growth at the hemispherical "ends" of a prolate spheroidal particle.

Interestingly, the standard deviations of the axial dimensions are substantially lower for particles seeded with 12-nm-diameter colloidal Au than for particles made by direct citrate reduction *or* 2.6-nm-diameter seeding For example, in batch 9 of the particles made by direct citrate reduction, the major axis is 56 ± 8.4

(22) (a) Creighton, J. A.; Blatchford, C. G.; Albrecht, M. G. *J. Chem. Soc., Faraday Trans. 2* **1979**, *75*, 790−798. (b) Blatchford, C. G.; Campbell, J. R.; Creighton, J. A. *Surf. Sci.* **1982**, *120*, 435−455.

(23) Bohren, C. F.; Huffman, D. R. *Adsorption and Scattering of Light by Small Paricles*; John Wiley & Sons: New York, 1983.

(24) Duff, D. G.; Curtis, A. C.; Edwards, P. P.; Jefferson, D. A.; Johnson, B. F. G.; Kirkland, A. I.; Logan, D. E. *Angew. Chem., Int. Ed. Engl.* **1987**, *26*, 676−678.

(25) Weisner, J.; Wokaun, A. *Chem. Phys. Lett.* **1989**, *157*, 569−575.

(26) Ahmadi, T. S.; Wang, Z. L.; Henglein, A.; El-Sayed, M. A. *Chem. Mater.* **1996**, *8*, 1161−1163.

(27) (A) Bard, A. J.; Faulkner, L. R. *Electrochemical Methods: Fundamentals and Applications*; John Wiley & Sons: New York, 1980. (b) Amatore, C. In *Physical Electrochemistry. Principles, Methods and Applications*; Rubinstein, I., Ed.; Marcel Dekker: New York, 1995; pp 131−208.

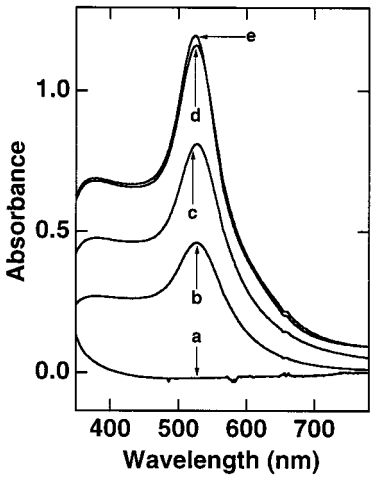


**Figure 3.** Optical spectra (0.1-s integration time) of a mixture of 3.2 mL of 0.01% $HAuCl_4$/0.1 mL of 40 mM $H_2NOH$ after 20 min (a), and 1 (b), 6 (c), 11 (d), and 56 s (e) after addition (without stirring) of 0.050 mL of 17 nM, 12-nm-diameter colloidal Au.

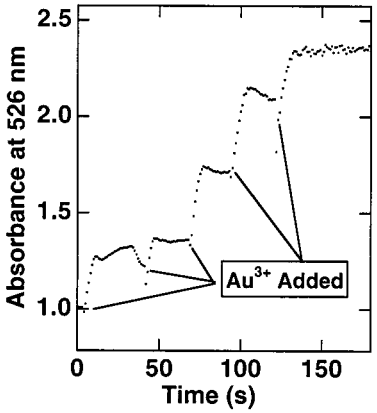


**Figure 4.** Absorbance at 526 nm measured every second (0.1-s integration time) after additions of 0.1 mL of 0.1% $HAuCl_4$ (at the times indicated) to an unstirred mixture of 3.2 mL of 0.01% $HAuCl_4$/0.1 mL of 40 mM $H_2NOH$/0.050 mL of 17 nM, 12-nm-diameter colloidal Au.

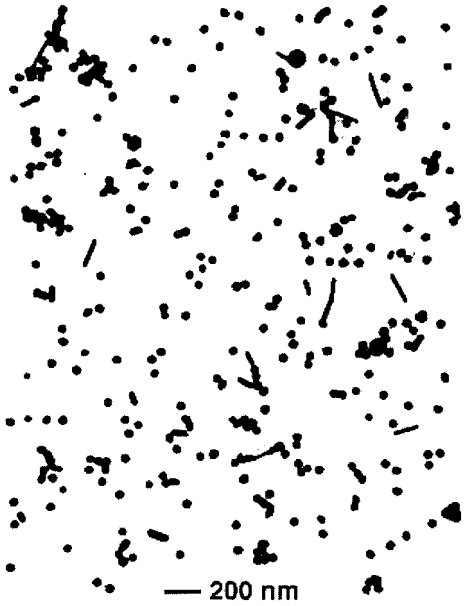


**Figure 5.** Representative TEM image of enlarged colloidal Au particles prepared by a two-step $NH_2OH$ seeding of colloidal Au (0.05 mL of 16.8 nM, 12-nm-diameter colloidal Au added to an unstirred mixture of 2.4 mL of 0.01%$HAuCl_4$/0.1 mL of 40 mM $NH_2OH$, then 0.1 mL of 1% $HAuCl_4$ added after ~2 min).

nm. For small seeds of the corresponding size (batch 5) $d = 56 \pm 7.2$ nm, while for batch 8 of the large seeds, $d = 53 \pm 4.8$ nm. The lower dispersity in particle size for 12-nm-seeded particles becomes even more significant for larger particles (e.g., large seed batch 9 vs small seed batch 6, large seed batch 10 vs small seed batch 7, and so on).

The increased dispersity in particle size for particles made using 2.6-nm diameter seeds simply reflects the poor monodispersity and increased ellipticity of the seeds themselves (Table 1 and Supporting Information). Despite many attempts, we have found that the 2.6-nm-diameter colloidal particles always have ~1-nm standard deviations in diameter. While this about the same absolute standard deviation in diameter measured for good preparations of 12-nm-diameter particles, it is quite large as a percentage of particle size. Furthermore, the measured ellipticity is 1.3 (versus 1.1 for 12-nm-diameter particles). Accordingly, seeding with 2.6-nm particles leads to more dispersion in particle size, reflected by larger standard deviations in diameter and by very substantial increases in peak widths (Table 1).

In short, citrate seeding 12-nm-diameter colloidal Au nanoparticles yields sols with improved physical properties relative to direct particle production by citrate reduction of $Au^{3+}$ or by seeding with 2.6-nm-diameter seeds. The disparity in quality of colloidal preparations is especially prevalent for $d > 40$ nm.

**Hydroxylamine Seeding.** Drawbacks of citrate seeding include the need for boiling $H_2O$ and the need to keep the $Au^{3+}$ and the reductant apart; ideally, seeding could be carried out at room temperature, and initiated upon introduction of seeds to premixed solutions of $Au^{3+}$ and reductant (or introduction of $Au^{3+}$ to a mixture of reductant and seeds). This can be accomplished by a process with a solution nucleation rate constant of zero at room temperature and a surface nucleation rate constant significantly greater than zero at room temperature. In Au electroless metal plating, these requirements are satisfied by chelation of $Au^+$ to cyanide, which moves the solution reduction potential too far negative for formation of $Au^0$, so that only adsorbed $Au^+$ ions is possible.[28] Similarly, the reductant hydroxylamine ($NH_2OH$) has previously been shown to favor reduction of Au ions at metallic Au surfaces at room temperature over reduction in solution,[14] and we have described in a preliminary fashion the application of $NH_2OH$ seeding to colloidal Au nanoparticles.[15]

At room temperature, mixtures of $NH_2OH$ and $Au^{3+}$ (added as $HAuCl_4$) do not lead to formation of colloidal Au nanoparticles in solution. Thus, the optical spectrum of a mixture of 0.01% $HAuCl_4$ and 40 mM $H_2NOH$ is featureless after 20 min (spectrum a of Figure 3). Addition of 50 $\mu$L of a solution containing 12-nm-diameter colloidal Au seeds leads immediately to significant growth in the intensity of the colloidal Au surface plasmon band (spectra b−e in Figure 3). Changes

(28) Kumar, A.; Biebuyck, H. A.; Whitesides, G. M. *Langmuir* **1994**, *10*, 1498−1511.

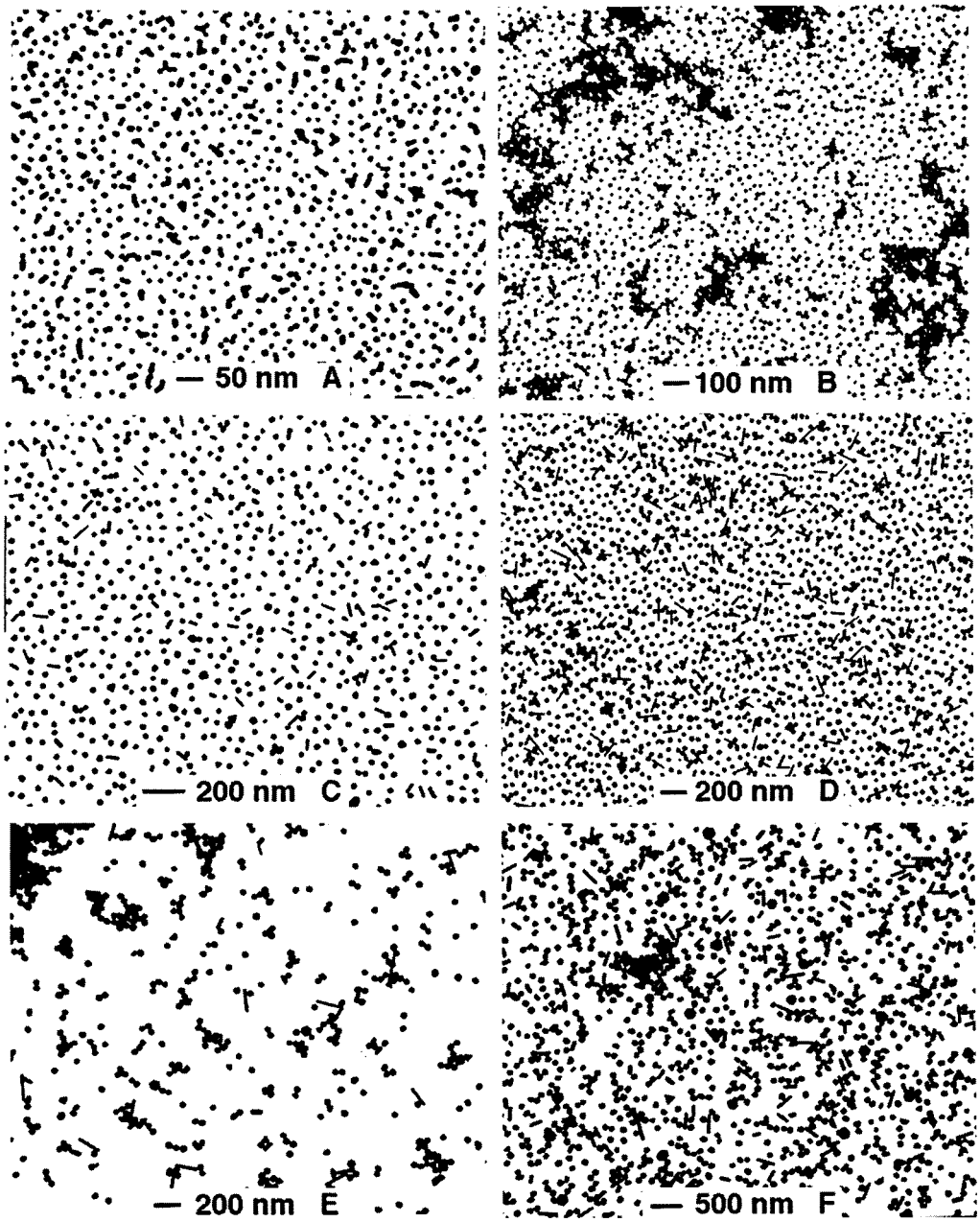


**Figure 6.** TEM images of colloidal Au grown by iterative $NH_2OH$ seeding. Major axis dimensions for spherical particles are as follows: 13 nm (panel A) [starting material]; 18 nm (panel B); 32 nm (panel C); 41 nm (panel D); 56 nm (panel E); and 116 nm (panel F). Detailed particle size analysis is given in Table 2; optical spectra and synthetic protocols for each set of particles are available in the Supporting Information.

in the optical spectra are essentially complete after 11 s, since a spectrum recorded after 56 s is essentially identical, as are spectra recorded every 5 s between these times (data not shown). Since the formation of new particles is precluded by the control experiment described by spectrum a, the spectral changes suggest enlargement of the seed particles. If so, cessation in particle growth must result from depletion of $Au^{3+}$.

This notion is confirmed by the data in Figure 4, which plots the absorbance at 526 nm over time as aliquots of $HAuCl_4$ are added to a prereacted mixture of 0.01% $HAuCl_4$, $NH_2OH$, and 12-nm-diameter colloidal Au. At $t = 0$, the absorbance $A \approx 1$, indicating that the $Au^{3+}$ already in solution has already been consumed to enlarge the 12-nm-diameter colloidal Au particles. After addition of $Au^{3+}$, there is a nearly instantaneous increase in absorbance,[29] followed by a slight decrease and then a leveling off. Each subsequent addition of $Au^{3+}$ leads to an increase in absorbance, and to a new (higher) level. Thus, $HAuCl_4$ can be made the limiting reagent in $NH_2OH$-seeded growth of 12-nm-diameter colloidal Au: introduction of a known quantity of $Au^{3+}$ to a solution containing colloidal Au nanoparticles and an excess of $NH_2OH$ leads to particle growth, until the $Au^{3+}$ is consumed.

This approach to seeded particle growth is attractive in three respects. First, particle enlargement can be carried out at room temperature. Second, since $Au^{3+}$ can be made limiting, it should be possible to grow particles

(29) The dips in the first seconds after each addition are due to the turbulence caused by pipet introduction into the cuvette.

**Table 2. Particle Size and Shape Analysis for Iteratively $NH_2OH$−Seeded Colloidal Au Nanoparticles**

| Figure 6 panel[a] | number sized | mean *d* major × minor[b,c] | median *d*[c] major × minor | *G* (mean) | predicted size[c,d] major × minor |
|---|---|---|---|---|---|
| | | Total[e] | | | |
| A | 1322 | 13.0 (1.4) × 11.8 (1.2) | 12.8 × 11.7 | 1.10 | |
| B | 2829 | 18.0 (2.7) × 16.3 (2.3) | 17.8 × 16.1 | 1.10 | |
| C | 2263 | 35.1 (9.0) × 28.4 (3.6) | 32.8 × 28.6 | 1.24 | |
| D | 3363 | 51.1(28.6) × 36.1 (5.4) | 41.7 × 37.0 | 1.42 | |
| E | 917 | 65.8(31.0) × 49.5 (7.0) | 56.0 × 49.9 | 1.33 | |
| F[f] | *g* | *g* | *g* | *g* | |
| | | Spheres[e] | | | |
| A | 1183 | 12.9 (1.3) × 11.9 (1.2) | 12.7 × 11.7 | 1.08 | |
| B | 2630 | 17.9 (2.5) × 16.4 (2.3) | 17.7 × 16.2 | 1.09 | 21.0 × 19.0 |
| C | 1964 | 32.4 (3.2) × 29.2 (2.7) | 32.3 × 29.0 | 1.11 | 33.7 × 30.3 |
| D | 2839 | 41.1 (4.0) × 37.7 (3.5) | 41.0 × 37.6 | 1.09 | 45.5 × 41 |
| E | 799 | 56.2 (5.4) × 51.0 (5.1) | 55.3 × 50.4 | 1.10 | 59 × 53 |
| F | 1443 | 116 (11) × 102 (10) | 116 × 102 | 1.14 | 121 × 103 |
| | | Rods[e] | | | |
| A | 120 | 14.2 (2.1) × 11.6 (1.7) | 13.7 × 11.2 | 1.22 | |
| B | 100 | 20.8 (4.3) × 15.1 (1.9) | 19.8 × 14.8 | 1.38 | |
| C | 200 | 58.9 (12.8) × 21.4 (3.2) | 57.3 × 21.0 | 2.75 | |
| D | 399 | 122 (32.2) × 25.3 (3.9) | 127.0 × 24.6 | 4.82 | |
| E | 80 | 145 (42.4) × 35.0 (7.0) | 163.5 × 33.0 | 4.14 | |
| F | 200 | 236 (60.3) × 77.1 (9.6) | 233.6 × 74.2 | 3.06 | |

[a] For convenience, solutions of seeded particles have been named according to their TEM image in Figure 6. [b] Numbers in parentheses refer to standard deviations. [c] In nanometers. [d] With the exception of B, whose predicted size was based on the actual size of A, predictions were based on predicted sizes from the previous iteration. [e] "Total" refers to all the particles in a given batch of colloid, while "spheres" and "rods" refer those subsets of particles possessing the corresponding shapes. Particles with $G > 1.2$ were called rods. [f] F represents a two-step iteration from E. The predicted dimensions for the hidden iteration (E′) was 84 × 72 nm. [g] The pronounced bimodality of the particle size distribution precluded meaningful calculation of mean diameter and ellipticity.

to a prespecified size. Finally, $NH_2OH/Au^{3+}$ seeding is well-suited for growth of immobilized Au nanoparticles, because a colloidal Au-derivatized surface can be easily immersed into a solution of $HAuCl_4/NH_2OH$.[15,30]

These advantages notwithstanding, the physical properties of $NH_2OH/Au^{3+}$-seeded colloidal Au particles ultimately determine the merit of this approach. Figure 5 shows a TEM image of colloidal particles produced by a $NH_2OH/Au^{3+}$ seeding procedure analogous to that described for the data in Figure 3. Two aspects of the image are striking: the excellent monodispersity of the spherical particles (51 ± 5.2 nm × 46 ± 4.7 nm), and the presence of a distinct population (5−10%) of colloidal Au rods (141 ± 38 nm × 31 ± 4.6 nm) with ellipticities far greater (∼4.5) than any particles derived from citrate reduction of $Au^{3+}$, whether seeded or not. The standard deviation of the major and minor axes of the spherical particles appears equivalent to that produced by citrate seeding with 12-nm-diameter colloidal Au. In contrast, the length of the rods' major axes is highly variable, ranging from 90 nm to >200 nm, while the rods' minor axes shows the same small standard deviation (4.7 nm) as the spherical particles. More importantly, the minor axis is more than three standard deviations shorter than the minor axis of the dominant population, suggesting that the rods do not form by fusion of spheres.

The origin of these rods is of great interest, particularly in view of theoretical prediction[6b] and of recent experimental confirmation[5a,b] of intense electromagnetic fields at the ends of highly prolate spheroids of Au and Ag. If the process of rod formation has a strong diffusional component (as described above for large colloidal Au nanoparticles made by the Frens method), it should be minimized by growing the particles in small steps (i.e., with limited $Au^{3+}$). If, on the other hand, the rods are formed by highly face-selective surface reactions, then stepwise growth will simply lead to stepwise rod expansion.

Iterative, stepwise seeding should also favorably impact the size and shape distribution of the spherical particles. Figure 1 and Table 1 show clearly that single-step enlargement of 2.6- or 12-nm-diameter colloidal Au particles diameters below 40 nm is well-behaved; for larger particles, the PWHM and ellipticity seem to rise exponentially. Growing large particles in multiple steps should lead to minimization of these effects.

The results of an iterative seeding experiment are shown in Figure 6, which depicts TEM images of the starting 12-nm-diameter seed particles and those resulting from five iterations, and in Table 2, a detailed particle size analysis. (The experimental protocols for iterative seeding and the optical spectra of the resulting colloidal Au solutions can be found in the Supporting Information.) Perusal of Figure 6, which shows spherical particles spanning nearly an order of magnitude in size (∼12−13 nm in panel A to over 100 nm in panel F) leads to two immediate conclusions. The first is that the colloidal Au rods are definitely not fused or aggregated spheres. This is easily confirmed by examination of Figure 7, an enlarged TEM image of panel E, which shows that the rods are solid and are significantly smaller in the minor axis than surrounding quasi-spherical particles. Another interesting point that can be gleaned from Figure 7 is that none of the rods are blunt-ended: both ends are hemispherical, some almost perfectly so. The second obvious finding from Figure 6 is that there is no continuum from spherical to rod-shaped particles; rather, there are two quite distinct populations, with nothing in between. Figure 8, a histogram showing the number of particles (in the colloidal preparation imaged in panel D) with a given

(30) Brown, K. R.; Natan, M. J. *Chem. Mater.* **2000**, *12*, 314−323 (subsequent paper in this journal).

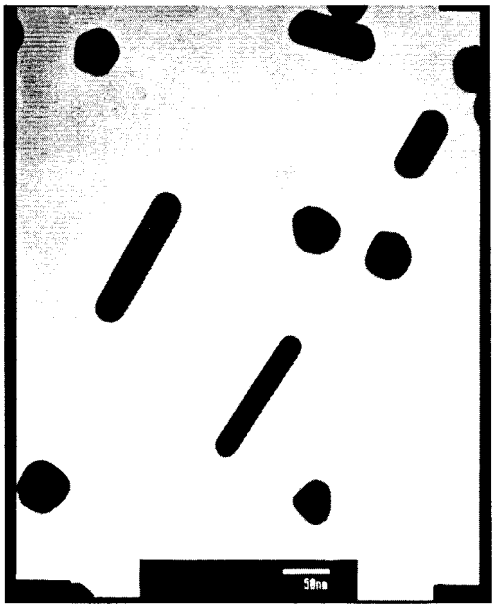


**Figure 7.** Enlarged TEM image of fourth iteration $NH_2OH$-seeded colloidal Au (panel E in Figure 6).

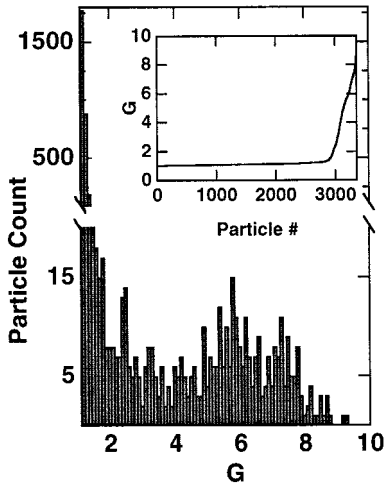


**Figure 8.** Histogram showing the number of particles exhibiting a given *G* for the Au colloid depicted in panel D of Figure 6. The same data are replotted in the inset, with each particle number based on sorted values of *G*.

*G* value, amplifies this point. The transition from $G < 1.5$ to $G > 1.5$ is extremely abrupt, with a 2 order of magnitude difference in particle populations. Equally revealing is the inset to Figure 8, a replotting of the same data based on sorted *G* values: nearly 3000 of the 3300 particles have a *G* close to 1, and the remainder have *G* values from 2 to as high as 8.

Table 2 gives size statistics for both particle shapes individually and for the total set of particles,[31] from which several key points are revealed. (i) Comparison of the median and mean values is provided to show that for samples containing a bimodal sample distribution, the statistical mean differs from the median value of the set. Likewise, the proximity of the median and mean values in small colloidal particle sets demonstrate that in a uniform particle set these two values should be close. (ii) The standard deviation (SD) of the axial dimensions also climbs very quickly. Once the rods are dropped from consideration, the SD for the remaining population drops dramatically and the median and mean values come into close agreement. (iii) Neither the 12 nm or the next larger colloid shows evidence of colloids with high G; the dominant population is spherical. However, the minor axis of the rods is substantially smaller than the minor axis of spheres in the same batch. Thus, the growth of 12-nm seed particles into rods must be a process that is not simply limited to an accelerated growth in one dimension but a reduced growth rate in the other two axial directions. Both these effects could derive from solution-phase transport/mixing phenomena causing a reduced flux of Au to the sides of the forming particle relative to the ends. Alternatively, a small population of the seed particles might exhibit substantially different properties, such as surface adsorbates, crystal faces, or lattice structure.

## Conclusions

Particle seeding appears to be a valuable addition to the synthetic repertoire for colloidal Au, both for the production of large particles with improved monodispersity and for fabrication of high aspect ratio colloidal Au rods. Both boiling citrate and room temperature hydroxylamine served effectively as reductants for 2.6- and 12-nm-diameter colloidal Au seeds. For hydroxylamine, iterative seeding can be used to grow (from 12-nm-diameter seeds) particles with 100−200-nm major axes. In our laboratories, the protocols reported herein have completely supplanted the more traditional approaches to syntheses of large-diameter colloidal Au nanoparticles; accordingly, these methods may be of general utility.

**Acknowledgment.** Support from NSF (CHE-9256692, CHE-9627338), NIH (GM55312-01), and the Beckman Foundation is gratefully acknowledged. Acknowledgment is also made to the Electron Microscopy Facility for the Life Sciences in the Biotechnology Institute at The Pennsylvania State University.

**Supporting Information Available:** TEM image of 2.6-nm diameter seeds, and optical spectra as well as synthetic protocols for the particles described in Figure 6 and Table 2. This material is available free of charge via the Internet at http://pubs.acs.org.

CM980065P

(31) For the smaller diameter particle sets, particularly **A**, assignment of the particles to the categories of rod or sphere is somewhat arbitrary, given the narrow size distribution and low ellipticiity. Accordingly, a *G* value of 1.2 was used as the cutoff for **A** and 1.3 was used for **B**.